CFD Modelling of 3-Way Catalytic Converters with Detailed Catalytic Surface Reaction Mechanism

Ming Chen, Joe Aleixo, Shazam Williams & Thierry Leprince
DCL International Inc.

Yi Yong
Fluent Inc.

ABSTRACT

This paper presents a 3-D CFD modelling of flow and heterogeneous reactions in catalytic converters. The pressure and velocity fields in the catalytic converters are calculated by the state of the art modelling technique for the flow resistance of catalyst substrate. A surface reaction model is applied to predict the performance of a three-way Pt/Rh catalyst. A reaction mechanism with detailed catalytic surface reactions for the 3-way catalyst is applied. The novelty of this approach is the use of a surface chemistry solver coupled with a 3-D CFD code in the entire computational domain of the catalyst substrate that allows flow distribution for complex configurations to be accounted for. The concentrations of the gas species and the site species are obtained. A comparison between the simulation results and the experimental data of a three-way catalyst was made.

INTRODUCTION

The performance map of a catalyst is mainly determined by precious metal loading, catalyst formulation, exhaust gas conditions and aging history. Fig. 1 is a modified diagram of the regimes of catalytic surface reactions based on [1], parameterized by the Damköhler number (defined in Appendix) and the exhaust gas temperature. Depending on the state of the catalyst and upstream exhaust gas conditions, a catalytic converter is operated in any of the following three reaction regimes:

1. In the intrinsic surface reaction regime, the Damköhler number is low, and the kinetics dominates over diffusion effects. The concentration gradients both in the washcoat pores and in the bulk gas are small.

2. In the significant pore diffusion regime, the concentration gradients in the pores become significant as a result of the diffusion through pore structures and surface reactions. Moderate gradients of concentrations in the bulk gas are formed.

3. The mass transfer regime corresponds to large Damköhler numbers. In this regime, the concentration gradients are very small within the pores, and are large within the boundary layer of the bulk gas. The reaction rate is limited by the mass transfer between the bulk gas and the outside surface of the washcoat.

Because of the complexity associated with the quantitative description of the interactions among catalytic surface reactions, mass diffusion, fluid dynamics and heat transfer, catalyst modelling relies heavily on experiments.
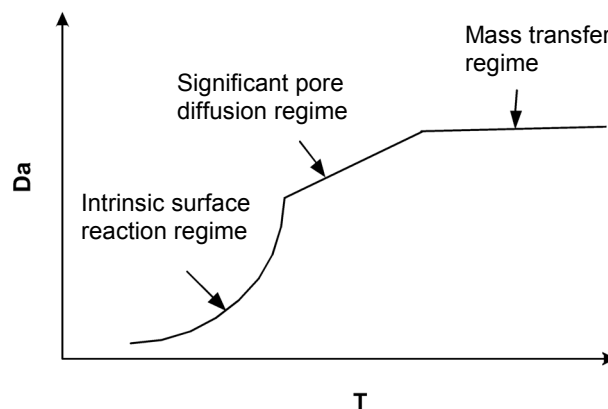
Fig. 1: Schematic of the regimes of catalytic surface reactions.

Chemical reaction kinetics is a key aspect in the modelling of catalyst performance. Models of reaction kinetics for catalytic converters may be divided into two categories: (1) Langmuir-Hinshelwood type with few global reaction steps [2,3,4], (2) detailed catalytic surface reaction mechanism [5,6,7].

In recent years, CFD simulation of catalytic converters using detailed catalytic surface reaction mechanisms has attracted interest, because it is believed that it allows a better prediction of the processes occurring in the converter, at extrapolated experimental conditions. Because a large amount of non-linear reaction

equations are included in the system, this approach requires a large computational capacity.

Chatterjee et al. [5] proposed a 3-way reaction mechanism through collection of the available rate constants, with some adjustment to fit the experimental data. This mechanism was applied in a transient numerical study using a concept of representative channels [7] where the modelling was done using a 3-D CFD code coupled with a 2-D surface reaction model. The detailed flow distribution in the substrate is smoothed or averaged.

In the present work, a surface chemistry solver coupled with a 3-D CFD code is used in the entire computational domain of the catalyst substrate. We attempt to validate the catalytic surface reaction model employed in FLUENT6.1.18 [8] with the reaction mechanism proposed by Chatterjee et al. For the purpose of flow calculation, the actual substrate is regarded as a porous medium and is treated as a fictitious continuum, such enabling the use of the partial differential equations in the whole computational domain. The effects of unresolved geometric surfaces of the channels in the substrate are included in the conservation equations for the species masses and energy. The porous medium assumption is a compromise to balance the complexity of the physics with the computational cost.

In the following the mathematical formulations for the sub-models employed in the present study are introduced. These sub-models deal with the flow resistance of substrates, the heat transfer between substrates and gas, and catalytic surface reactions. Furthermore, specific simulation examples are provided to illustrate the applicability of these models.

MODELLING OF THE CATALYTIC CONVERTER

FLOW RESISTANCE OF THE SUBSTRATE

The flow resistance coefficients of substrates are anisotropic and are practically deduced from experiments. They are specified along three directions based on the substrate type, the cell density, the hydraulic diameter and the resistance of the substrate.

The empirical expression for calculating local pressure drop reads:

$$\Delta P = a \; \mu \; \frac{L}{d_h^2} \; v + \frac{1}{2} \; Y \; \rho_g \; v^2 \tag{1}$$

The resistance coefficient of the substrate, Y, is a function of cell density, substrate material and coating thickness. In the employed CFD software package, FLUENT [8], porous media are modeled by the addition of source terms to the momentum equations of flow. The source term for the i th momentum equation reads:

$$\frac{\partial p}{\partial x_i} = -\sum_{j=1}^{3} D_{ij} \mu \, v_j - \frac{1}{2} \sum_{j=1}^{3} C_{ij} \rho \mid v_j \mid v_j \tag{2}$$

When the direction of the i th coordinate coincides with the longitudinal direction of substrate channels, one obtains the following expressions of the viscous resistance coefficient (D) and the inertial resistance coefficient (C):

$$D_{ii} = a/d_h^2 \tag{3}$$

$$D_{jj} = D_{kk} = +\infty \tag{4}$$

$$C_{ii} = Y/L \tag{5}$$

$$C_{jj} = C_{kk} = +\infty \tag{6}$$

The non-diagonal components of the matrices C and D are zero. Here the subscripts j and k denote the other two coordinate directions of a Cartesian coordinate system. For a better convergence of the numerical solution, D_{jj} and D_{kk}, C_{jj} and C_{kk} are practically assumed as 1000 times of D_{ii} and C_{ii}, respectively. Table 1 summarizes the flow resistance coefficients of a metallic substrate with different cell density. Eqs. (5) and (6) are only valid for a flow-through substrate with no flow through the walls.

Table 1. Flow resistance coefficients, L = 0.09 m.

cell density (cpsi)	200	300	400
C_{ii} [m^{-1}]	8.48	8.66	8.91
D_{ii} [m^{-2}]	1.25×10^7	1.78×10^7	2.74×10^7

HEAT TRANSFER BETWEEN SUBSTRATE AND EXHAUST GAS

The energy equation of gas phase and the energy equation of solid phase are coupled by a heat transfer coefficient:

$$h = Nu \, \lambda_g / d_h \tag{7}$$

Here the Nusselt number Nu is assumed as a constant following [11]. In FLUENT a dual cell mesh technique is employed which allows a cell based heat transfer between the gas phase and the solid phase within the concept of porous medium treatment.

MODELLING OF CATALYTIC SURFACE REACTIONS

Reaction Mechanism - Following [5], a surface reaction mechanism for a Pt/Rh three-way catalyst is applied, which consists of 60 elementary reaction steps and one global reaction step, involving 8 gas species and 23 site species. It includes the steps of adsorption of the reactants on the active sites of the surface, reaction of the adsorbed species, and desorption of the reaction products. The mechanism consists of three parts: (1) a mechanism of C_3H_6 oxidation on Pt/Al$_2$O$_3$, (2) a mechanism of NO reduction on Pt, (3) a mechanism for NO reduction and CO oxidation on Rh. The standard formation enthalpies of the adsorbed species are taken from [12].

<u>Surface Reaction Model</u> - The heterogeneous reaction is of the general form

$$\sum_{i=1}^{N_g} g_{i,r}^{'} G_i + \sum_{i=1}^{N_s} s_{i,r}^{'} S_i \rightarrow \sum_{i=1}^{N_g} g_{i,r}^{''} G_i + \sum_{i=1}^{N_s} s_{i,r}^{''} S_i \qquad (8)$$
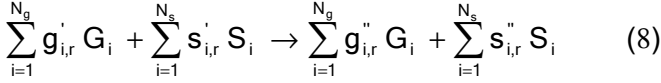
where G_i and S_i represent the gas species and the site species (adsorbed species), respectively. The rate of r th forward reaction reads:

$$R_r = k_{f,r} \prod_{i=1}^{N_g} [G_i]_{wall}^{g_{i,r}^{'}} [S_i]_{wall}^{s_{i,r}^{'}} \qquad (9)$$

The forward rate constant for r th reaction, $k_{f,r}$ is given by

$$k_{f,r} = A_r \, T^{\beta_r} \exp\left(-\frac{E_r}{RT}\right) \qquad (10)$$

A_r is adjustable due to surface site coverage. The latter is defined as the fraction of surface sites covered by the species. Because of the original implementation of the code and lack of data, the coverage dependence of the rate constant is accounted for by an ad hoc expression

$$E_r = E_{r,0} - \sigma \, \Theta_i \qquad (11)$$

Here $E_{r,0}$ is the activation energy taken from the original reaction mechanism, σ is an adjusting parameter, and Θ_i the surface coverage of species i. The above expression is only applied for few selected critical reaction steps.

For adsorption reactions, the rate constant is calculated by

$$k_{f,r}^{ads} = \frac{S_i^0}{\Gamma^\tau} \sqrt{\frac{RT}{2\pi \, Mw_i}} \qquad (12)$$

Where S_i^0 is the initial sticking coefficient. Γ is the surface site density, and τ is the number of sites occupied by the adsorbing species.

The concentration of the site species i is given by

$$[S_i]_{wall} = \Gamma \, \Theta_i \qquad (13)$$

Since the creation or depletion of species through heterogeneous reactions must be balanced by the mass flux through the surface, one obtains:

$$\rho D_i \frac{\partial Y_{i,wall}}{\partial n} = \eta \, F \, Mw_i \, \hat{R}_{i,gas} \quad i = 1, 2, 3, \cdots, N_g \qquad (14)$$

For unresolved surfaces, the term on the l. h. s. of Eq. (14) can be expressed as $k_{m,i} \rho (Y_i - Y_{i,wall})$. Here $k_{m,i}$ is the mass transfer coefficient. The mass diffusivity of the

species, D_i, is temperature dependent, and is calculated following [10]. F is the ratio between catalytic surface and geometric surface. Because the local concentration gradients in the washcoat pores are not numerically resolved, the effectiveness factor, η, is introduced to take account of the effects of pore diffusion in the washcoat. The effectiveness factor is dependent on pore tortuosity, washcoat thickness, mass diffusivity, concentrations of gas phase at the washcoat and intrinsic surface reaction rates [1]. The effectiveness factor is estimated by a simplified analytical solution of a catalyst with CO as species [1].

The variation of the surface coverage is given by

$$\Gamma \frac{\partial \Theta_i}{\partial t} = \hat{R}_{i,site} \qquad i = 1, 2, 3, \cdots, N_s \qquad (15)$$

$\hat{R}_{i,gas}$ and $\hat{R}_{i,site}$ are the net reaction rates of the gas species and site species, respectively.

$$\hat{R}_{i,gas} = \sum_{r=1}^{rxn} (g_{i,r}^{''} - g_{i,r}^{''}) R_r \qquad i = 1, 2, 3, \cdots, N_g \qquad (16)$$

$$\hat{R}_{i,site} = \sum_{r=1}^{rxn} (s_{i,r}^{''} - s_{i,r}^{''}) R_r \qquad i = 1, 2, 3, \cdots, N_s \qquad (17)$$

RESULTS AND DISCUSSIONS

CASE STUDY OF FLOW CHARACTERISTICS IN CATALYTIC CONVERTERS

In order to use a multi-dimensional CFD code to simulate heterogeneous reactions in practical conditions, one first needs to predict the flow field in the exhaust pipes, cones and catalyst substrates. In the following, the flow characteristics for a typical catalytic converter are numerically investigated.
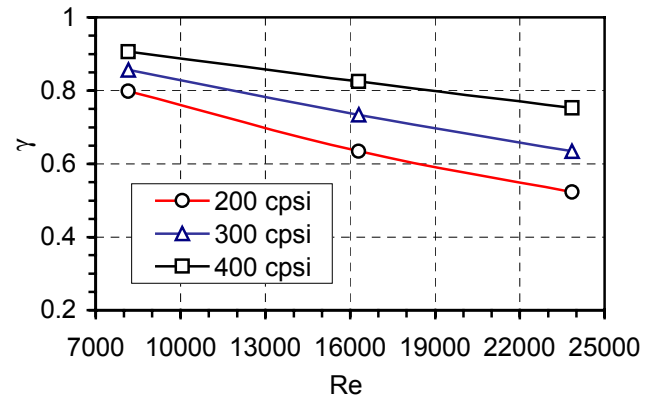
Fig.2: The calculated flow uniformity index, γ, at the front face of the substrate. Both the Reynolds number and the cell density are varied. The substrate is metallic. The flow resistance coefficients are taken from Table 1.

A cylindrical metallic substrate with a length of 9 cm and a diameter of 7.6 cm is connected to two cones with a cone angle of 45°. The inlet and outlet pipe diameters

are 1/3 of the substrate diameter, respectively. The Reynolds number, which is based on the inlet pipe diameter, is varied from 8000 to 24000. The exhaust gas has a temperature of 700 K. The outer walls are assumed adiabatic. The flow in the substrate, which is represented by a porous zone, is laminar. The flow in the remaining part of the domain is turbulent. The turbulence is modeled by the standard k-ϵ turbulence model. The mesh consists of 93000 non-uniform hexahedral cells.
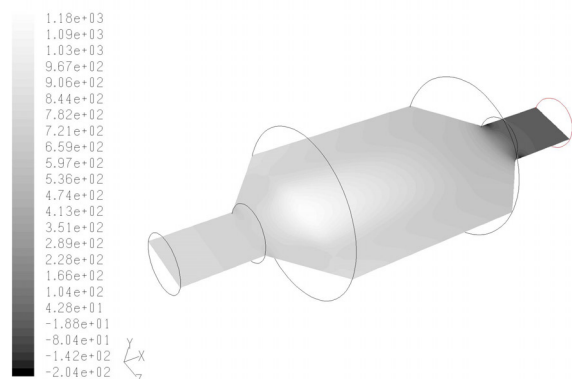
Fig. 3: The contours of the static pressure on a cross section. The cell density is 300 cpsi, and the Reynolds number is 16000.
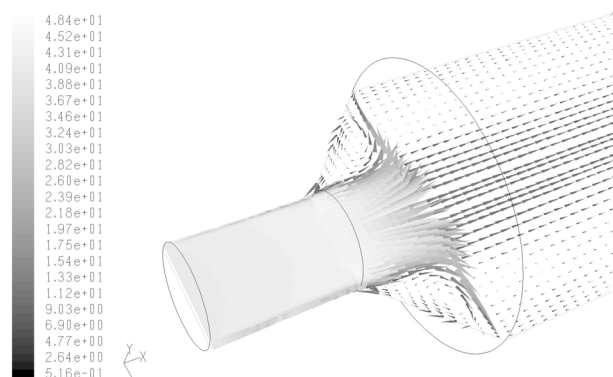
Fig. 4: The velocity vectors on the cross section. The cell density is 300 cpsi, and the Reynolds number is 16000.

The flow in the catalytic converter is determined by the geometrical configuration, the flow resistance characteristic of the substrate and the Reynolds number. Fig. 2 indicates that the calculated flow uniformity index at the front face of the substrate is decreased with the increasing of the Reynolds number, and increased with the increasing of the cell density. Fig. 3 and Fig. 4 show the contours of the static pressure and the velocity vectors at a cross section, respectively. It is shown that a large recirculation zone is formed in the diffuser. When the flow enters the porous zone, it aligns with the channel direction. The higher pressure is located around the catalyst entrance and the centre line.

CASE STUDY OF CATALYTIC SURFACE REACTIONS

<u>Geometry and Boundary Conditions</u> - A comparison is made between the simulated catalyst performance and the experimental data. The latter was obtained by a test on a laboratory-scale tube reactor [5, 9]. A catalyst, as summarized in Table 2, is located in the tube. The inlet and outlet faces are located 10 mm upstream and downstream of the catalyst, respectively. Fig. 5 shows the geometry and computational domain. The compositions of the nearly stoichiometric mixture are given in Table 3. The inlet flow is assumed as uniform, and the gas velocity is 1.35 m/s evaluated at 300 K, which corresponds to a space velocity of 168,000 1/h. The flow in the porous region and the other fluid zones are laminar. The inlet gas temperature is varied from 500 K to 800 K.

Fig. 5: The geometry and the surface mesh.

Table 2. Catalyst data [5].

Precious metal loading	50 g/ft^3, Pt/Rh = 5:1
Substrate material	cordierite
Cell density	400 cpsi
Washcoat material	ceria stabilized γ -alumina
Substrate length	29 mm
Substrate diameter*	10 mm
Surface site density	2.72 X 10^{-9} mol/cm^2
Geometric surface area per unit volume	2740 m^2/m^3
Ratio of active metal surface and geometric surface	70

 * The diameter of the substrates is defined by the authors.

Table 3. Volumetric inlet concentrations of the species.

CO	1.42 [%]
O$_2$	0.77 [%]
C$_3$H$_6$	0.0450 [%]
NO	0.1000 [%]
N$_2$	Balance

Results and Discussions - In Fig. 6, the calculated conversion efficiencies of CO, NO and C_3H_6 are shown as a function of the inlet temperature for the mixture in Table 3. The conversion of CO, NO and C_3H_6 begins at 550 K. At the temperature of 700 K, the conversion efficiencies reach the maximum values. The calculated conversion of CO is 88% at 800 K, which is consistent with the concentration of O_2 in the mixture.
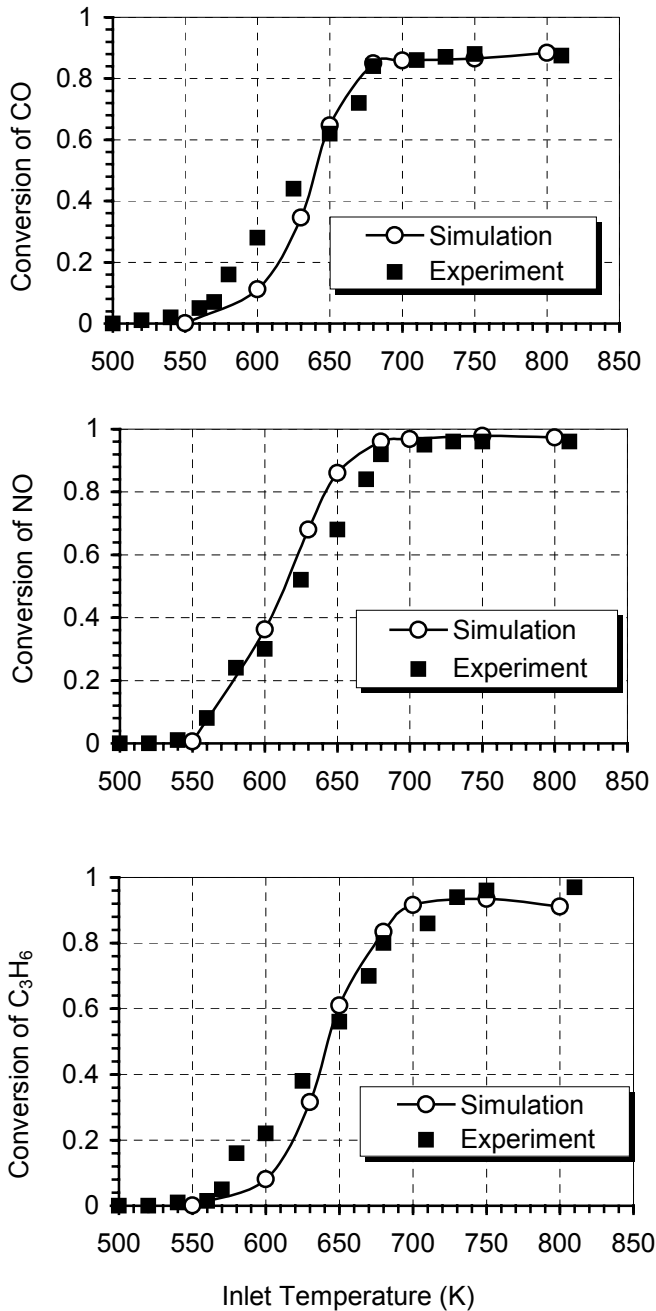
Fig. 6: The conversion efficiency of CO, NO and C_3H_6. The experimental data are from [5,9].

Mass fraction of CO

Mass fraction of CO_2

Mass fraction of NO

Mass fraction of C_3H_6
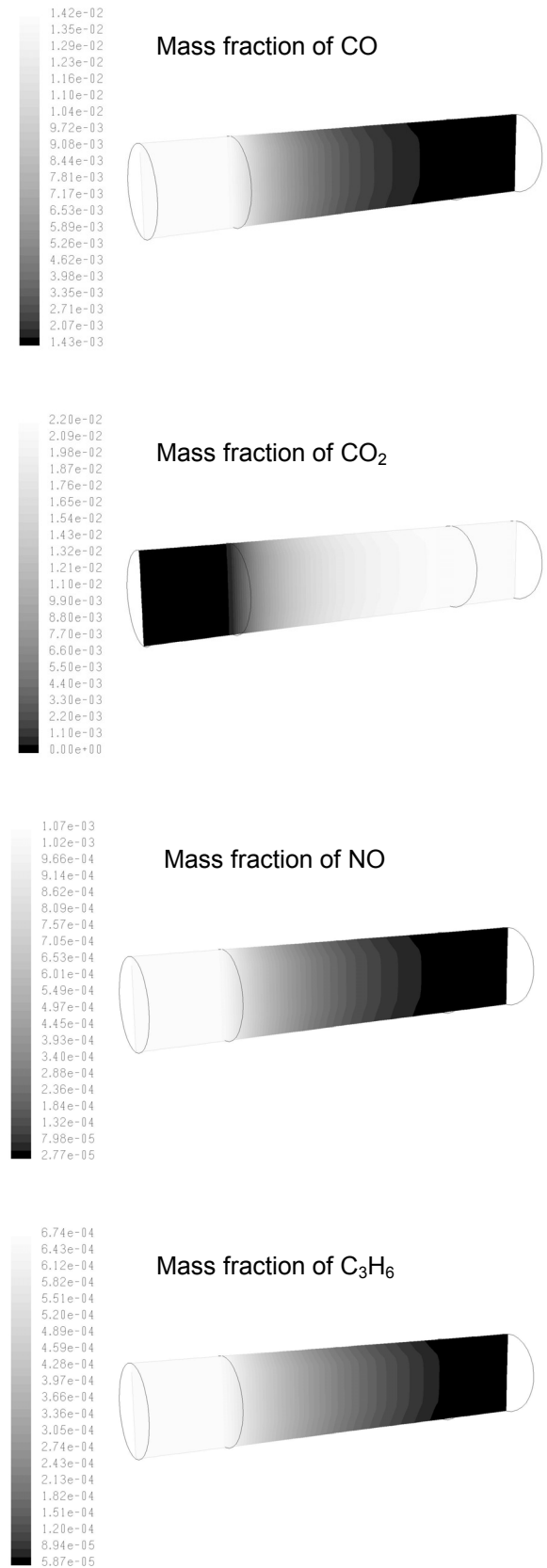
Fig. 7: The contours of the mass fractions of CO, CO_2, NO and C_3H_6 at 800 K.
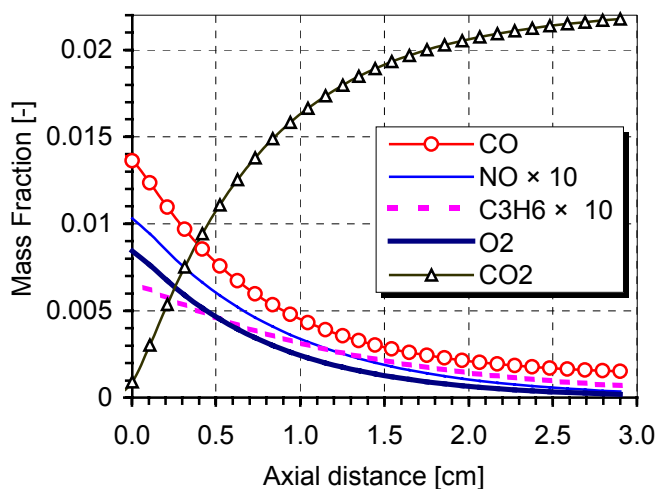
Fig. 8: The mass fractions of CO, NO, C_3H_6 , O_2 and CO_2 along the centre line of the catalyst, at 800 K.

There is a competition between CO and C_3H_6 for O_2. In the temperature range between 750 K and 800 K, there is a slight increase of the calculated conversion efficiency of CO, accompanied by a slight decrease of the conversion efficiency of C_3H_6. The under-estimation of the C_3H_6 conversion at 800 K could be corrected by a tuning of the kinetics parameters. The NO is completely converted at 750 K. The calculated light-off curves agree well with the experimental data, especially at high temperature.

Fig. 7 shows the contours of the mass fractions of CO, CO_2, NO and C_3H_6 at the inlet gas temperature of 800 K. The mass fractions of CO, CO_2, NO, C_3H_6 and O_2 along the centre line of the catalyst are shown in Fig. 8. For the same case, the coverage of CO(s) on Pt is varied from 0.2 to 0.3. The O(s) coverage on Pt is decreased along the centre line. The Pt(s)/O(s) ratio is large because of the low oxygen concentration in the gas phase. The Rh surfaces are mainly covered with N(Rh). Along the centre line of the catalyst, the N(Rh) coverage is decreased, and the number of free Rh sites is increased.

CONCLUSION

The presented numerical study shows that the flow field in the catalytic converter is influenced by the flow resistance of the substrate for a given geometric configuration and at a given Reynolds number. The numerical examples indicate that the flow uniformity index at the front face of the substrate is decreased with the increasing of the Reynolds number, and increased with the increasing of the cell density.

A surface reaction model with moderate sophistication is applied to predict the performance of a three-way catalyst. The comparison between the present 3-D steady state CFD solutions and the experimental data shows that the conversion efficiencies for the interested species are reasonably predicted using the surface reaction model with the detailed reaction mechanism.

REFERENCES

1. Charles N. Satterfield, Mass Transfer in Heterogeneous Catalysis, Robert E. Krieger Publishing Company, Inc., 1981.
2. S. E. Volt, et al., Kinetics Study of Carbon Monoxide and Propylene Oxidation on Platinum Catalysts, Ind. Eng. Chem. Prod., Res. Dev., **12**, 294, 1973.
3. S. H. OH and J. C. Cavendish, Mathematical Modelling of Catalytic Converter Lightoff, AIChE Journal, Vol. 31, No. 6, 1985, pp. 935-949.
4. G. C. Koltsakis, P. A. Konstantinidis, A. M. Stamatelos, Development and Application of Mathematical Models for 3-way Catalytic Converters, Applied Catalysis B: Environment, Vol. 12, 1997, pp. 161-191.
5. D. Chatterjee, O. Deutschmann and J. Warnatz, Detailed Surface Reaction Mechanism in a Three-Way Catalyst, Faraday Discuss., 2001, **119**, p. 371-384.
6. O. Deutschmann, R. Schmidt, F. Behrendt and J. Warnatz, Numerical Modelling of Catalytic Ignition, Twenty-Sixth Symposium (International) on Combustion, The Combustion Institute, 1996, pp. 1747-1754.
7. J. Windmann, J. Braun, P. Zacke, et al., Impact of the Inlet Flow Distribution on the Light-Off Behavior of a 3-Way Catalytic Converter, SAE paper 2003-01-0937.
8. FLUENT 6.1.18, FLUENT Inc.
9. J. Braun, T. Hauber, H. Többen, P. Pazke, D. Chatterjee, O. Deutschmann and J. Warnatz, Influence of Physical and Chemical Parameters on the Conversion Rate of a Catalytic Converter: A Numerical Simulation Study, SAE paper 2000-01-0211.
10. D. E. Rosner, Transport Processes in Chemically Reacting Flow Systems, Butterworths, 1986.
11. S. Siemund, D. Schweich, J. P. Leclerc and J. Villermaux, Modelling Three-Way Monolithic Catalytic Converter: Comparison Between Simulation and Experimental Data, Catalysis and Automotive Pollution Control, III, Studies in Surface Science and Catalysis, Vol. 96, 1995.
12. D. Chatterjee, Detaillierte Moderllierung von Abgaskatalysatoren, Ph.D. Thesis, Heidelberg University, Germany, 2001.

CONTACT

E-Mail: mchen@dcl-inc.com
Website: www.dcl-inc.com

η	internal effectiveness factor [-]
μ	dynamic viscosity [kg/(m·s)]

DEFINITIONS, ACRONYMS, ABBREVIATIONS

a	entrance loss coefficient [-]
A_r	pre-exponential factor [mol, m, s]
C	inertial resistance coefficient [m^{-1}]
D	viscous resistance coefficient [m^{-2}]
D_i	mass diffusivity of species i [m^2/s]
Da	Damköhler number [-]
d_h	hydraulic diameter of the substrate [m]
E_r	activation energy [J/kmol]
F	ratio between catalytic surface and geometric surface
g	stoichiometric coefficient for gas species [-]
$[G_i]_{wall}$	molar concentration of gas species i on surface
h	heat transfer coefficient [J/(m^2·s·K)]
$k_{m,i}$	mass transfer coefficient [m/s]
L	length of catalyst [m]
M_w	molecular weight [kg/kmol]
N	number of species [-]
n	normal distance from cell centre to wall [m]
p	static pressure [Pa]
Δp	drop of static pressure [Pa]
v	superficial gas velocity [m/s]
R	universal gas constant [J/kmol·K]
$\widehat{R}_{i,gas}$	net reaction rate of gas species [kmol/m^2·s]
$\widehat{R}_{i,site}$	net reaction rate of site species [kmol/m^2·s]
Re	Reynolds number based on the diameter of inlet pipe
s	stoichiometric coefficient for site species [-]
S^0	initial sticking coefficient [-]
$[S_i]_{wall}$	molar concentration of site species i on surface
t	time [s]
T	temperature [K]
x	coordinate [m]
Y	resistance coefficient of the substrate [-]
Y_i	mass fraction of gas species [-]
$Y_{i,wall}$	mass fraction of gas species at the wall of substrate

Greek symbols

β_r	temperature exponent [-]
γ	flow uniformity index [-]
Θ	surface coverage [-]
Γ	surface site density [kmol/m^2]
ρ	density of gas [kg/m^3]
λ	thermal conductivity of gas [W/(m·K)]

Subscript

g	gas; gas species
s	solid; site species
r	index of reaction step
rxn	number of reactions
wall	solid surface of substrate
i	species index; index of the coordinate
j	index of the coordinate
k	index of the coordinate

Superscript

ads	adsorption
'	reactant
''	product

APPENDIX

γ VALUE

The flow uniformity index, γ, is defined by

$$\gamma = 1 - \sum_{i=1}^{N} \frac{|v_i - \overline{v}|}{2\overline{v}X} X_i$$

where v_i is the local gas velocity in the cell i, and $\overline{v}$ is the average gas velocity. X_i is the area of cell i, and X is the cross section area. N is the number of the cells in the cross section.

DAMKÖHLER NUMBER

The Damköhler number is defined by

$$Da = \frac{k \cdot L}{v}$$

where k is the overall rate constant [s^{-1}].